

# Long-term supplementation with anthocyanin-rich or -poor *Rubus idaeus* berries does not influence microvascular architecture nor cognitive outcome in the APP/PS-1 mouse model of Alzheimer's disease

Aaron Alonso Torrens, Christopher A. Mitchell, L. Kirsty Pourshahidi, Brian Óg Murphy, William Allwood, Lisa Rizzetto, Matthias Scholz, Kieran Tuohy, Gema Pereira-Caro, José Manuel Moreno-Rojas, Gordon McDougall & Chris I. R. Gill

To cite this article: Aaron Alonso Torrens, Christopher A. Mitchell, L. Kirsty Pourshahidi, Brian Óg Murphy, William Allwood, Lisa Rizzetto, Matthias Scholz, Kieran Tuohy, Gema Pereira-Caro, José Manuel Moreno-Rojas, Gordon McDougall & Chris I. R. Gill (2022): Long-term supplementation with anthocyanin-rich or -poor *Rubus idaeus* berries does not influence microvascular architecture nor cognitive outcome in the APP/PS-1 mouse model of Alzheimer's disease, International Journal of Food Sciences and Nutrition, DOI: [10.1080/09637486.2022.2141209](https://doi.org/10.1080/09637486.2022.2141209)

To link to this article: <https://doi.org/10.1080/09637486.2022.2141209>



© 2022 The Author(s). Published with license by Taylor & Francis Group, LLC.



[View supplementary material](#)



Published online: 30 Nov 2022.



[Submit your article to this journal](#)



Article views: 397







[View related articles](#)



[View Crossmark data](#)

## Long-term supplementation with anthocyanin-rich or -poor *Rubus idaeus* berries does not influence microvascular architecture nor cognitive outcome in the APP/PS-1 mouse model of Alzheimer's disease

Aaron Alonso Torrens<sup>a</sup>, Christopher A. Mitchell<sup>a</sup>, L. Kirsty Pourshahidi<sup>a</sup> , Brian Óg Murphy<sup>a</sup>, William Allwood<sup>b</sup> , Lisa Rizzetto<sup>c</sup>, Matthias Scholz<sup>c</sup>, Kieran Tuohy<sup>c</sup>, Gema Pereira-Caro<sup>d,e</sup>, José Manuel Moreno-Rojas<sup>d,e</sup>, Gordon McDougall<sup>b</sup>  and Chris I. R. Gill<sup>a</sup> 

<sup>a</sup>Nutrition Innovation Centre for Food and Health (NICHE), Centre for Molecular Biosciences, University of Ulster, Coleraine, Northern Ireland, UK; <sup>b</sup>Plant Biochemistry and Food Quality Group, Environmental and Biochemical Sciences, The James Hutton Institute, Invergowrie, Dundee, Scotland; <sup>c</sup>Nutrition and Nutrigenomics Unit, Research and Innovation Centre, San Michele all'Adige, Trentino, Italy; <sup>d</sup>Department of Food Science and Health, Andalusian Institute of Agricultural and Fisheries Research and Training (IFAPA), Alameda del Obispo, Córdoba, Spain; <sup>e</sup>Foods for Health Group, Instituto Maimónides de Investigación Biomédica de Córdoba (IMIBIC), Córdoba, Spain

### ABSTRACT

Disruption of microvascular architecture is a common pathogenic mechanism in the progression of Alzheimer's disease (AD). Given the anti-angiogenic activity of berry (poly)phenols, we investigated whether long-term feeding of *Rubus idaeus* (raspberries) could ameliorate cerebral microvascular pathology and improve cognition in the APP/PS-1 mouse model of AD. Male C57Bl/6J mice (50 wild type, 50 APP/PS-1) aged 4-months were fed for 24-weeks, with a normal diet enriched with either 100 mg/day glucose (control diet) or supplemented with glucose and freeze-dried anthocyanin-rich (red) or -poor (yellow) raspberries (100 mg/day) and assessed/sampled post intervention. Cerebral microvascular architecture of wild-type mice was characterised by regularly spaced capillaries with uniform diameters, unlike APP/PS-1 transgenic mice which showed dysregulated microvascular architecture. Long-term feeding of raspberries demonstrated limited modulation of microbiota and no substantive effect on microvascular architecture or cognition in either mice model although changes were evident in endogenous cerebral and plasmatic metabolites.

### ARTICLE HISTORY

Received 26 September 2022  
Accepted 25 October 2022

### KEYWORDS


Alzheimer's disease; transgenic mice; raspberries; polyphenols; anthocyanins; cognition; microvasculature

### Introduction

Alzheimer's disease (AD) is the most common cause of dementia, clinically characterised by difficulties with planning, reasoning, judgement and memory (Khan et al. 2016). Accumulation of amyloid- $\beta$  (A $\beta$ ) protein and phosphorylated tau aggregates in the brain parenchyma resulting in neuronal loss and synapse degeneration (Serrano-Pozo et al. 2011) are no longer considered the sole causes of the progression in pathophysiology. A growing body of evidence implicates cerebrovascular diseases (CVD) as a contributing factor in the development of AD (Lamar et al. 2020; Hendrickx et al. 2021), with dysbiotic microbiota also reported in both AD patients and recognised AD models (Elmaleh

et al. 2021). This may in part be due to the gut microbiota's important role in regulating barrier function, both locally and in other organ systems. Consequently, disturbance of the gut-brain axis is reflected in blood-brain barrier (BBB) and microbiome dysfunction thought to presage the neuroinflammation and plaque formation that precedes AD (Rutsch et al. 2020). In addition, several studies have shown that disruption of the BBB and impaired cerebral blood flow (CBF) results in the accumulation of A $\beta$  in the brain (Bookheimer et al. 2000; Knopman and Roberts 2010). Angiogenesis, or the growth of capillaries from pre-existing vessels, can contribute to A $\beta$  accumulation in AD as hypoxia, inflammation and increased oxidative stress accompanies the production of small-diameter tortuous vessels with low

**CONTACT** Christopher A. Mitchell  Ca.mitchell@ulster.ac.uk; Chris I. R. Gill  c.gill@ulster.ac.uk  Nutrition Innovation Centre for Food and Health (NICHE), Ulster University (Coleraine), Cromore Road, Coleraine, Co. Londonderry BT52 1SA, Northern Ireland, UK

 Supplemental data for this article can be accessed online at <https://doi.org/10.1080/09637486.2022.2141209>.

© 2022 The Author(s). Published with license by Taylor & Francis Group, LLC.

This is an Open Access article distributed under the terms of the Creative Commons Attribution-NonCommercial-NoDerivatives License (<http://creativecommons.org/licenses/by-nc-nd/4.0/>), which permits non-commercial re-use, distribution, and reproduction in any medium, provided the original work is properly cited, and is not altered, transformed, or built upon in any way.

rates of flow (Jefferies et al. 2013). Pathological angiogenesis is a hallmark of impaired CBF in a range of mouse models of AD (Beckmann et al. 2003) and a recognised feature of cerebral AD pathology in post-mortem studies of human brain (Pfeifer et al. 2002). Furthermore, the presence of A $\beta$  in APP mutant mouse models of AD has been reported to significantly alter brain vasculature; for example, APP23 mice show alterations in blood flow as well as structural modification of blood vessels. Similar microvascular pathologies are also observed in 3-month-old and 27-month-old mice after ultrastructural analysis (Beckmann et al. 2003). The importance of such microvascular alterations and their implications for AD pathogenesis and therapy have been comprehensively reviewed by Steinman et al. (2021).

Yet, despite AD being a leading cause of death worldwide, the majority of treatments, excluding the recently approved use of Aducanumab for AD-related mild cognitive impairment (Herring et al. 2021), provide only symptomatic relief and show little evidence of prevention or delay of disease progression (Srivastava et al. 2021). The lack of effective pharmaceutical intervention and nature of the disease has resulted in a significant economic burden to society (Wimo et al. 2017). Epidemiological evidence indicates that there are protective effects on cognitive decline (Morris et al. 2015; Berendsen et al. 2018) and lower risk of AD (Román et al. 2019) associated with the Mediterranean diet. Polyphenols are likely to be important mediators of such dietary effects, with high polyphenol take, specifically flavanols, anthocyanins and flavonoid polymers, being associated with lower AD risk (Shishtar et al. 2020). In pre-clinical and clinical studies, polyphenol-rich foods such as berries may be a viable option to prevent the early cognitive decline that is associated with progression of AD (Gildawie et al. 2018; Lamport and Williams 2021) given that consumption of anthocyanin-rich blueberries are associated with improved cognitive performance in older adults (Miller et al. 2018; Rutledge et al. 2021). These health effects appear, at least in part, to work through the gut microbiota and microbiota modulatory components (e.g. probiotics, prebiotic fibres and polyphenols) as all have been reported to reduce inflammation, improve barrier function and reduce A $\beta$  formation in AD pre-clinical models (Fan et al. 2021; Wu et al. 2020; Go et al. 2021; Cao et al. 2021; El Gaamouch et al. 2021). Moreover, flavonoids like taxifolin found in berries can increase blood flow and limit A $\beta$  production in the brain (Saito et al. 2017). Major components of berries such as anthocyanins inhibit angiogenesis (Tsakiroglou et al. 2019) and

anthocyanin-rich extracts inhibit vessel formation over time in a concentration-dependent manner (Joshua et al. 2017).

Consequently, the main objectives of this study were to determine if a diet supplemented with anthocyanin-rich (red) and -poor (yellow) raspberries can restore wild-type cerebral microvascular morphology in the APP/PS-1 mouse model of AD and protect against cognitive decline and whether this is via modulation of the gut microbiota and metabolic output.

## Material and methods

Anthocyanin-rich (red) and -poor (yellow) *Rubus idaeus* varieties were selected for the current study, red raspberry (Glen Ample) and the yellow raspberry variety (Hutton breeding line 08108H1). The raspberries were grown at the James Hutton Institute (Scotland, UK) in 2016, picked when ripe and frozen on the day of harvest then freeze dried and then milled to less than 0.5 mm particle size. The freeze-dried powder was individually portioned (10 g) for use in study and stored at  $-80^{\circ}\text{C}$ .

## Raspberry composition

The red and yellow raspberry powders (200 mg) were extracted using 1 ml of a mixture of methanol:distilled water (80:20, v/v) with 1% formic acid (FA). The mixture was sonicated for 15 min and then centrifuged at 4900 rpm for 10 min. The supernatant was collected and frozen at  $-80^{\circ}\text{C}$  until analysis. The analysis of individual anthocyanins, ellagic acid derivatives and other phenolics was carried out using an UHPLC Dionex Ultimate 3000 system (Thermo Scientific, San José, USA) on a quaternary Rs Pump and autosampler (Dionex Ultimate 3000) and coupled to an Exactive mass spectrometer with heated-electrospray ionisation probe (HESI). The separation was performed on a SB-C18 ( $2.1 \times 100$  mm,  $1.8 \mu\text{m}$ ) column set at  $40^{\circ}\text{C}$  (Agilent, Santa Clara, USA) and at 0.4 ml/min. The solvents used as mobile phase were: Solvent A (water/FA 95:5, v/v) and solvent B (acetonitrile/FA 95:5, v/v), in the following gradient: 0–2 min, 5% B; 2–12 min from 5% to 100% B; 12–13 min from 100% to 5% B and then, 5% B up to 15 min. MS data were acquired in negative mode for phenolic acids, flavonoids and other phenolics and in positive mode for anthocyanins by full scan acquisition covering  $m/z$  100–2000 at 30,000 resolution. HESI source parameters were: source voltage 3.5 kV, tube lens voltage 50 V, capillary temperature  $300^{\circ}\text{C}$  and sheath and auxiliary gas flow

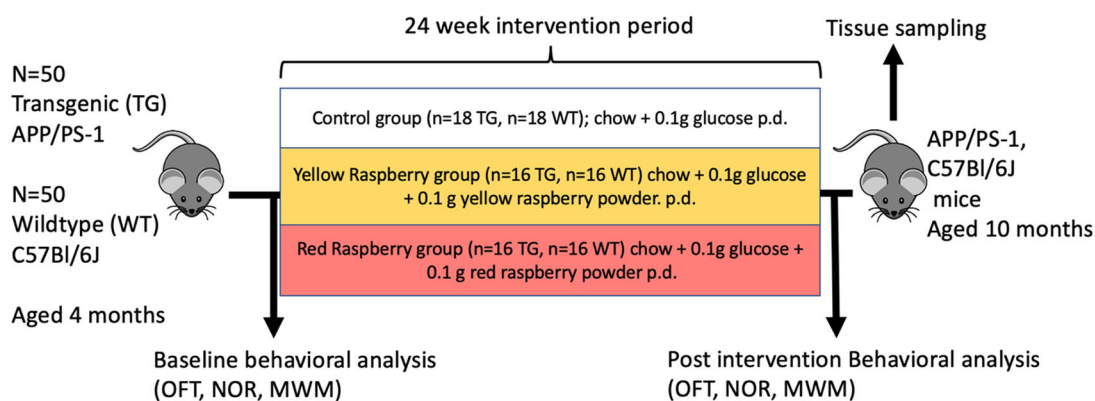


**Figure 1.** Study design. Four-month-old APP/PS-1 (TG) and wild-type (WT) littermates ( $n = 100$ ) were fed a normal rodent diet (Teklad Global 16% Protein Rodent Diet, Envigo) supplemented with either 0.1 g *p.d.* glucose only (Controls:  $n = 18$  TG, 18 WT), glucose mixed with *Rubus* powder (0.1 g *p.d.*) from either red or yellow raspberries ( $n = 16$  TG, 16 WT per group) for 24 weeks. Behavioural assessment was conducted pre and post intervention using open field test (OFT) novel object recognition tests (NOR) and Morris water maze (MWM). Tissue sampling occurred at 10 months.

rate ( $N_2$ ) 45 and 20 (arbitrary units). Identification of (poly)phenols was performed by comparing the exact mass and the retention time with available standards. In the absence of standards, components were tentatively identified by comparing the theoretical exact mass with the measured accurate mass of the molecular ion. Quantification was carried out by obtaining the peak areas under the theoretical exact mass of the molecular ion and comparison to standard curves. In the absence of standards, compounds were quantified by reference to the calibration curve of a related compound. No ellagitannin standards were available so their levels were compared by peak areas.

### Animals

This study received local and UK Home Office ethical approval and was conducted in accordance with the Animals (Scientific Procedures) Act of 1986. The mice were housed in a room maintained at 22 °C with a 12:12 light:dark cycle. A total of 100 male mice, 50 C57Bl/6J and 50 expressing APP/PS1 mutation in both the APP and presenilin gene, were bred with C57BL/6 female mice (Harlan, Blackthorn, UK). After 21 days, offspring were weaned and tested for baseline cognitive testing at 4 months of age in seven different cohorts of 10–16 mice. Mice were genotyped through polymerase chain reaction (PCR) using ear tissue samples and primers specific for the APP-sequence (Kelly et al. 2017). Six-month-old APP/PS-1 and wild-type littermates were fed a normal rodent diet (Teklad Global 16% Protein Rodent Diet, Envigo) supplemented with either 0.1 g *p.d.* glucose only (Controls:  $n = 36$ ), glucose mixed with *Rubus* powder (0.1 g *p.d.*)

from either red or yellow raspberries ( $n = 32$  per group) for 24 weeks (Figure 1).

### Tissue sampling

Microvascular corrosion casting: upon conclusion of study and all cognitive assessment (described later), six mice from each group were selected at random for microvascular casting studies as described in Kelly et al. (2015). In brief, the selected mice were anaesthetised (isoflurane), an incision around the abdomen was then made exposing the diaphragm and rib cage. The diaphragm was then cut and the rib cage was clamped. A catheter was then introduced via the right ventricle into the aorta, being tied up with a 5-0 suture. The right atrium was then cut allowing proper flushing of the vascular system with 10–15 ml phosphate buffer solution at 37 °C, followed by 10–15 ml injection of 2.5% glutaraldehyde (Sigma-Aldrich, UK). 15 ml of PUII resin compound was then used allowing microvasculature casting. Following complete polymerisation (12 h at room temperature), the brain was removed and desiccated for further SEM analysis.

The remaining mice not selected for casting were terminally exsanguinated and approximately 1 ml of heparinised blood was collected on ice. Samples were centrifuged at 13000 rpm for 10 min, then plasma samples were aliquoted and stored –80 °C for subsequent metabolomic analysis. Brains were removed from mice and bisected horizontally through the mid-sagittal plane into each hemisphere from which one lobe was used for subsequent metabolomic analysis. Faecal pellets were collected directly from the intestine and immediately frozen in liquid nitrogen for metagenomics analysis.



### Non-targeted LC-MS<sup>n</sup> analysis

Brain tissue was weighed and homogenised in glass hand-held homogeniser using 1 ml of ice-cold extractant A [methanol containing 0.5% (v/v) FA and 20 mM diethyl dithiocarbamate (DDC)]. A second 1 ml was added, and homogenisation repeated. The solution was poured into 13 ml labelled tubes and stored on ice. 1 ml of extractant B (ultra-pure water containing 0.5% (v/v) FA and 20 mM DDC) was added to the homogeniser and the material was homogenised again. After storage on ice for 15 min, the samples were centrifuged (15 min, 2500 × g, 5 °C) and supernatants decanted into new fresh labelled tubes. The supernatants were stored at −80 °C overnight to precipitate proteins and centrifuged again. 1.8 ml of each sample was pipetted into 2 ml Eppendorff tubes and dried from frozen in a Speed-Vac.

Serum samples were thawed from −80 °C storage and 500 µL samples were pipetted into labelled 2 ml tubes. 1 ml of extractant A was added, vortexed well and placed in −80 °C freezer overnight. After centrifugation in pre-chilled microfuge (10,500 × g, 5 °C, 15 min), 1000 µL was removed from each sample into 2 ml tubes and dried in Speed-Vac from frozen. When required, material was re-suspended in 50 µL of acetonitrile then vortexed well. 200 µL of 0.1% FA in UPW containing the internal standard compound, morin, at required final concentration was added to each sample and vortexed again. Samples were placed into LC-MS filter vials. The metabolic profiles of the brain and plasma samples were analysed by LC-MS<sup>n</sup> using an Orbitrap MS in both positive and negative ionisation modes as described previously (McDougall et al. 2017). The extraction efficiency was assessed by doping in morin, epicatechin and quercetin in mice brain and serum samples at 10 µM then following the extraction procedure above. The recoveries were all > 90%.

### Data handling and statistical analysis for non-targeted analysis

The LC-MS data from the samples from the control and raspberry fed animals were converted into MZML centroid format using the Proteowizard MSConvert software package (<http://proteowizard.sourceforge.net/>). The data were then deconvoluted using the XCMS online package (<https://xcmsonline.scripps.edu/>) producing a Microsoft Excel based XY matrix of the paired RT and *m/z* of each feature against the peak intensity for each sample. The dataset was next subjected to automated peak annotation workflows within

PutMedID (Brown et al. 2011; Allwood et al. 2013), highly correlated (Pearson 0.9>) *m/z* features within a set RT window are grouped and considered as *m/z* likely associated with the same compound (i.e. a ‘peak group’). Accurate mass differences between *m/z* within each peak group were next calculated to allow the annotation of the parent *m/z*, isotope and adduct ions, as well as common in-source fragments. The neutral accurate mass was then matched to a library of possible metabolite features and associated metabolites (Plant Metabolic Network PlantCyc database (<http://www.plantcyc.org/> and the Manchester Metabolomics Database (MMD: <http://dbkgroup.org/MMD/>)). After annotation, non-grouped low intensity features, redundant isotope, adduct and fragment features were removed from the dataset to reduce data complexity.

### Gut microbiome analysis

Total DNA was extracted from faecal samples (8–10 mg) using the FastDNA<sup>TM</sup> SPIN Kit for Faeces (MP Biomedicals, Santa Ana, CA, USA). PCR amplification was performed using the bacterial specific primer set 341 F (5' CCTACGGGNGGCWGCAG 3') (Klindworth et al. 2013) and 806 R (5' GACTACN VGGGTWTCTAATCC3') with overhang Illumina adapters targeting a ~460 bp fragment of the 16S rRNA variable region V3-V4 and used for community 16S rRNA partial gene sequencing by Illumina<sup>®</sup> MiSeq (PE300) platform (MiSeq Control Software 2.0.5 and Real-Time Analysis software 1.16.18) as previously described (<https://pubmed.ncbi.nlm.nih.gov/28538678/>).

Initial processing of sequence data, quality control, phylotype binning and taxonomic alignment of raw sequencing reads were performed using DADA2 (Callahan et al. 2016) and follow-up statistical analyses were performed using the QIIME software, version 1.9.1 (Caporaso et al. 2010). After quality control processing, sequencing resulted in a total of 3,520,369 rDNA reads with a mean of 49,582.662 (± SD 12,003.741) OTU-like [amplicon sequence variants (ASVs)] per sample accounting for a mean of 386.507 ± 66.174 ASVs per sample. Taxonomy assignments were performed using the SILVA 132 reference database (Quast et al. 2013). Starting from a table of ASVs we obtained the final output from metagenome prediction as an annotated table of predicted gene family counts for each sample. Alpha (within-sample richness) and beta-diversity (within and between-

sample Bray-Curtis dissimilarity) estimates were computed using QIIME software.

### Behavioural assessment

Open field test (OFT). Mice were placed in the centre of the arena and allowed to explore the open field for 5 min. Motor activity (path length), exploratory behaviour (rearing), anxiety level (grooming session), speed and time spent in the centre versus the periphery of the arena was then monitored and recorded.

Novel Object Recognition task (NOR) was taken place in a circular open field where movements throughout the trial were recorded. Working memory was further assessed by subjecting mice to a 10 min acquisition period, with two identical objects NOR. Following a 3–4 h retention period mice were re-exposed for 10 min to one of the previously encountered objects and a 'novel' object that the animal had not previously explored. The discrimination score for novel object exploration was calculated by the recognition index (RI). The RI was calculated for each object, defined as the amount of time spent exploring object A or B over the total time spent exploring both objects  $\times 100$  ( $tA$  or  $tB / (tA + tB) \times 100$ ).

### Morris water maze

Spatial learning was measured in the Morris water maze (MWM) task. Mice were handled for 2 min and 30 s for 2 weeks previous to the test, allowing them to adapt to conditions previously mentioned. A circular pool with a hidden platform was used and mice learned the location using visual cues. The acquisition phase involved 4 trials per animal at 90 s max for 4 days. On the fifth day, the probe trial was conducted the object being to determine whether or not the animal remembered where the platform was located (memory recall). Mice were given 60 s to swim in the pool without the platform. The time spent in the target quadrant of the pool or the other three quadrants (opposite target quadrant, clockwise or counterclockwise from target quadrant) was then compared between groups to estimate memory recall of the mice).

### Statistical analysis

Data are expressed as groups mean  $\pm$  SD unless otherwise indicated. For metabolomic analysis, Principal component analysis (PCA) was applied to the XCMS data from all subjects (SIMCA-P 12.0.1.0 software)

and separation was noted between the samples from the control fed, and the red and yellow raspberry fed mice. Therefore, discriminant optimised partial least squares (OPLS-DA) analysis was also justified. Using the loadings plot from the OPLS-DA analysis, a list of putative metabolites was extracted that most influenced the separation towards the raspberry-fed samples. Components were then putatively identified by their MS properties and possible molecular formulae generated in the XCMS process and checked against literature. For cognitive tests, analysis was conducted using one-way ANOVA. Differences were considered significant at  $p \leq 0.05$  including where Tukey comparison tests were performed for correction analysis. For microbiome analysis, the non-parametric Kruskal–Wallis test was used for the comparison of relative abundances of microbial taxa between groups, and the resulting  $p$ -values were corrected (Bonferroni correction) for multiple testing controlling the false discovery rate (Benjamini and Hochberg 1995) at all taxonomic levels taken into account.

## Results

### Composition of raspberries

The red raspberries were almost 12-fold higher in total quantifiable (poly)phenol content (Table 1) than the yellow raspberries and this difference was predominantly due to the low anthocyanin content of the yellow variety. The phenolic acid, flavonol and catechin and the ellagic acid derivatives only made up a small portion of the total polyphenol content in the red raspberries. The ellagitannins, Sanguiin H6 and Lambertianin C were also noted as major components but were not quantified as no suitable standard was available. However, the levels of these ellagitannins as

**Table 1.** Comparison of (poly)phenolic composition of red and yellow raspberries.

Components ( $\mu\text{g/g}$ DW)	Yellow raspberry		Red raspberry	
	Mean	SE	Mean	SE
Phenolic acids	324.20	37.24	453.80	81.70
Flavonols and catechins	1514.70	25.20	1200.40	49.01
Ellagic acid derivatives	230.10	20.27	167.10	35.91
Cyanidin-3-sophoroside	237.70	9.01	15218.20	830.77
Cyanidin-3-(2'- <i>O</i> -glucosyl)rutinoside	78.90	3.00	3068.10	201.73
Cyanidin-3-glucoside	202.30	9.30	4707.50	428.64
Cyanidin-3-rutinoside	54.50	2.66	3474.50	300.58
Cyanidin-xylosyl-rutinoside	ND	ND	40.50	2.77
Pelargonidin-3- <i>O</i> -sophoroside	4.90	0.17	310.00	44.40
Pelargonidin-3- <i>O</i> -glucoside	0.00	0.00	321.00	28.46
Cyanidin-3, 5- <i>O</i> -diglucoside	46.40	2.42	3609.60	369.46
Delphinidin-3- <i>O</i> -glucoside	40.10	2.83	25.90	2.08
Anthocyanins	664.80	29.39	30,775.30	2208.89
Total polyphenol ( $\mu\text{g/g}$ DW)	2733.80	203.29	32,632.40	2375.51

Mean of triplicates; ND, not detected, under the limit of quantification.

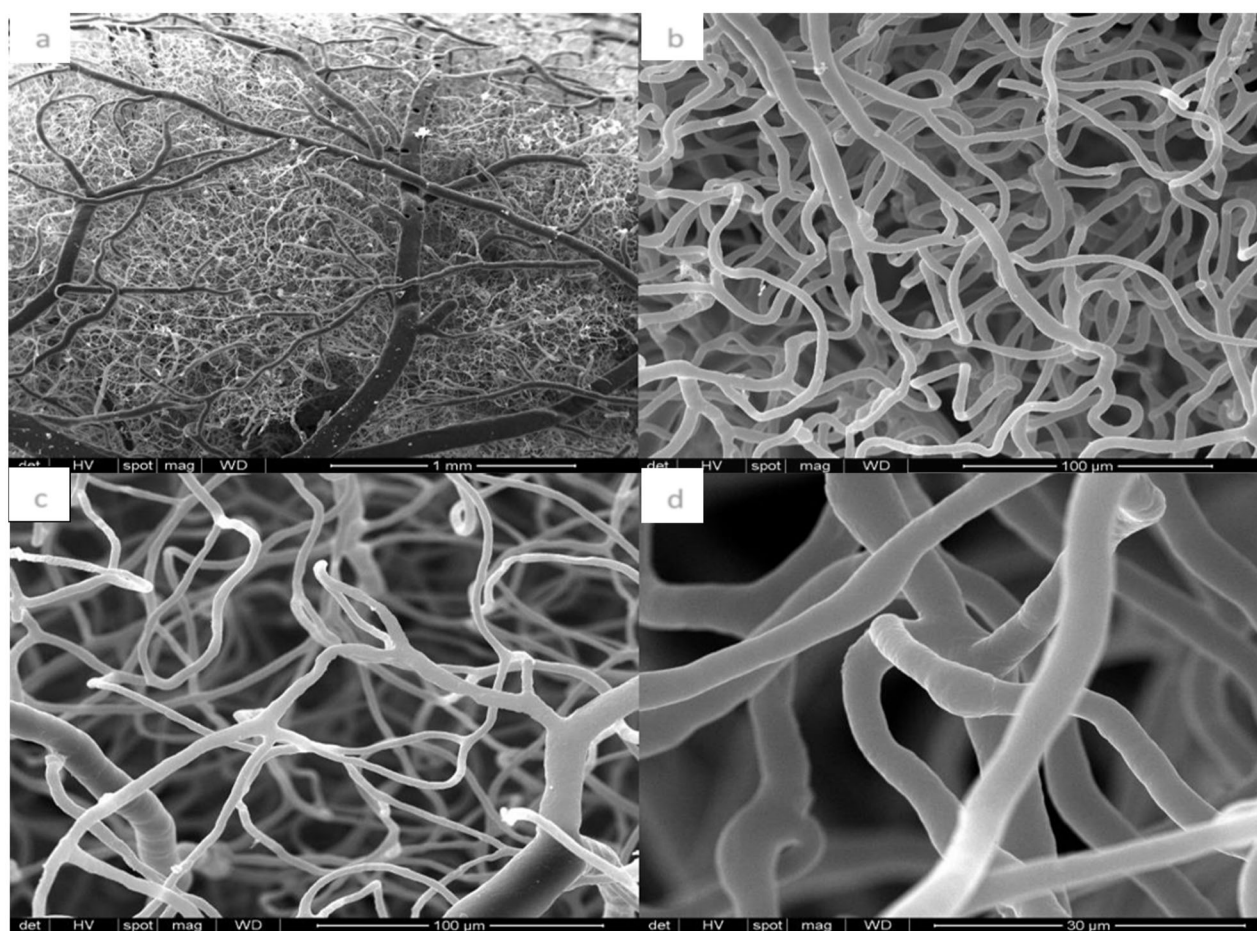


**Figure 2.** SEM of microvascular corrosion casts from the cerebral hemisphere of a wild-type C57Bl/6J mouse fed with control diet. (a) At low power, this part of the surface of the cerebral hemisphere shows superficial veins and venous sinuses (with pitted surfaces) overlaying a network of smaller diameter capillaries. Occasional, rarified areas of vasculature are also observed, particularly close to large vessels. In (b), small venules with smooth surface contours drain a network of evenly spaced capillaries which (c) periodically bend at  $\sim 90^\circ$ : a conspicuous feature of cerebral microvasculature, which ensures regional perfusion. (d) High-resolution ultrastructural analysis reveals capillaries with diameters between 3 and 5  $\mu\text{m}$ , with fine surface textural features and rarely, small eccentrically located bulges are observed (d).

assessed by MS peak areas was also slightly higher in the red raspberries (e.g.  $\sim 117\%$ ,  $p < 0.005$ ). The red raspberries also had higher levels of total carotenoids ( $164.87 \pm 0.26 \mu\text{g/g DW}$ ) compared with the yellow raspberries ( $72.79 \pm 0.26 \mu\text{g/g DW}$ ;  $p < 0.001$ ), whereas the yellow raspberries had significantly higher vitamin C content than the red raspberries ( $2.91 \pm 0.06$  vs.  $2.62 \pm 0.04 \text{ mg/g DW}$ , respectively;  $p < 0.001$ ).

#### **Corrosion cast ultrastructure in wild-type mice**

Cerebral cortex microvascular morphology in wild-type control-fed mice was characterised by regularly spaced capillaries with uniform diameters and smooth surfaces (Figure 2). The smallest capillaries in wild-type mice were 3–5  $\mu\text{m}$  in diameter and typically bend along their length at least once by up to  $90^\circ$  (Figure 2b,c), a feature that is characteristic of plexus architecture in wild-type

murine cerebral microvessels. Larger diameter surface veins or arterioles were regularly spaced on the cerebral cortex, between flattened venous sinuses (Figure 2a). Occasional areas within the cortical surface (particularly near large veins or venous sinuses) were conspicuously devoid of capillaries (Figure 2a). Very rarely, capillaries in the wild-type mice contain microaneurisms, visible as small bulges in the vessel surface (Figure 2d). In yellow raspberry fed (Figure 3) and red raspberry fed mice (not shown), microvessel architecture was identical in appearance to control mice.

#### **Corrosion cast ultrastructure in APP/PS-1 transgenic mice**

Low power SEM images in the cerebral cortex of APP/PS-1 mice supplemented with control feed revealed a variety of aberrant microvessel morphological features,



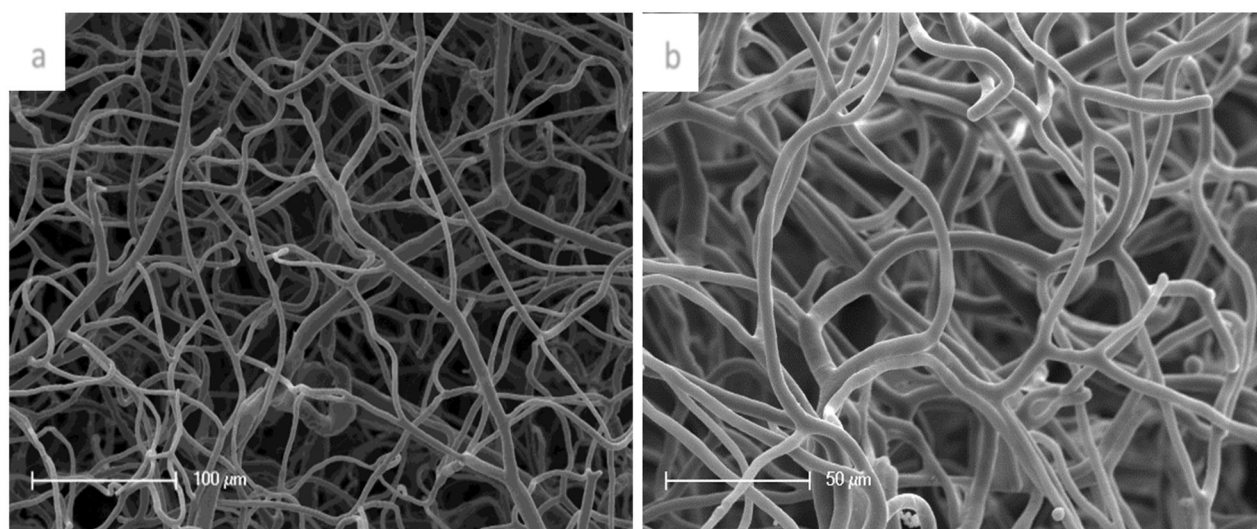


**Figure 3.** Microvascular corrosion cast SEM images of the cerebral microvasculature from a wild-type animal supplemented with freeze-dried yellow-raspberry for 6 months. (a) Small calibre veins, drain a regularly spaced network of capillaries. (b) The capillaries have smooth luminal surfaces and show no evidence of microaneurisms or inter-endothelial leakage of resin. Typical cerebral microvessel spacing is approximately 50 µm and the gaps between segments is consistent.

that were characteristic of this strain of transgenic animal (Kelly et al. 2015, 2017). These include increased frequency and extent of rarefied capillary areas giving the surface a ‘moth-eaten’ appearance as well as larger calibre vessels with widely variant vessel diameters (Figure 4a). Higher power images of microvessel plexi in these mice clearly showed roughened capillary surfaces (Figure 4b) and wide variation in diameters of arterioles (Figure 4c). Capillaries were frequently clustered (Figure 4a; a sign of recent angiogenesis), exhibited roughened surfaces with non-uniform diameters (Figure 4b,c). Some capillaries had distinctive irregular and bulbous granular distensions of the vessel wall (Figure 4d) similar to those described in previous studies of APP/PS-1 transgenic mice (Kelly et al. 2015, 2017).

In APP/PS-1 mice supplemented with either yellow (Figure 5) or red (Figure 6) raspberry, a range of cerebral microvascular pathologies were observed. Capillary clusters as well as vessel poor regions were observed within the cerebral cortex of APP/PS-1 mice receiving yellow berry supplementation (Figure 5a,b). Irregular, bulbous distensions of the capillary wall were frequently seen (Figure 5a,b), in addition to rectangular tags on endothelial surfaces consistent with leakage of resin between inter-endothelial junctions. In addition, thin flattened microvessels, consistent with incomplete capillary formation, were conspicuous in areas with capillary clusters indicative of recent angiogenic vessel formation. In some SEM images, microvessel loss in APP/PS-1 mice supplemented with yellow berries was severe, microvessel clustering was

obvious and inter-endothelial leakage was conspicuous (Figure 5b). Similarly, low power imaging of brains from APP/PS-1 supplemented with red berries revealed cerebral microvasculature with numerous vessel-poor areas, capillary clustering and evidence of failed angiogenesis (Figure 6a,b). Higher power images of microvasculature from these mice showed evidence of failed sprouting angiogenesis and clustering of angiogenic capillary segments around larger vessels. Despite detailed examination of vascular casts from APP/PS-1 mice treated with either yellow or red raspberry, there were no significant changes in microvascular architecture in these animals compared with those supplemented with the control diet.

#### **Effects of raspberry consumption of metabolomic profiles in brain and plasma**

LC-MS<sup>n</sup> data were obtained from each sample type in both negative and positive ionisation modes as some metabolites are only readily detectable in one ionisation mode. Metabolomic profiles from samples of brain contained many identifiable metabolites (Supplementary Table S1), but substantial inter-individual variation was evident for metabolomic profiles of mice within the same feeding regimes (e.g. Supplementary Figure S1 = control fed mice; Supplementary Figure S2 = red raspberry and Supplementary Figure S3 = yellow raspberry fed mice). Consequently, identification of metabolites consistently and significantly different between different feeding regimes in both brain and plasma samples was challenging (Supplementary Figures S4–S6).



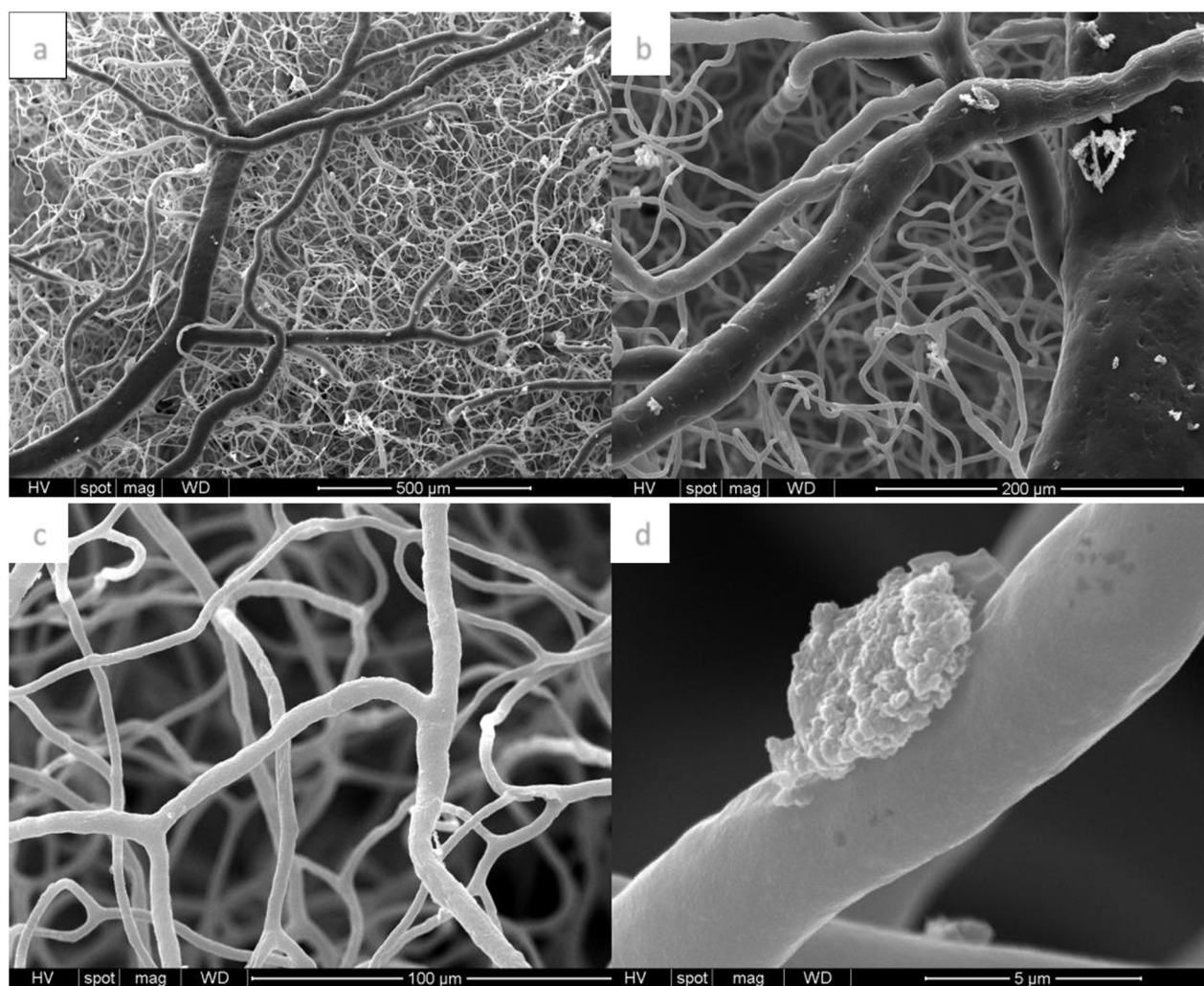


**Figure 4.** Microvascular corrosion cast SEM images of the cerebral hemispheres of an APP/PS1 tg mouse fed with control diet. (a) At low power, superficial venous sinuses (flattened vessels with pitted and dimpled surface) overlay a microvascular network with numerous gaps devoid of capillaries (c.f. wild-type control-vehicle) and intertwined capillary networks, giving the overall architecture a 'moth eaten' appearance. The (white) flocculent materials (in a and b) are artefactual remnants of cellular debris from insufficient washing following the maceration process. In (a), a cerebral venous sinus (right) with two surrounding arterioles are conspicuous, one of which is severely narrowed 100  $\mu\text{m}$  upstream of its bifurcation point (a typical feature of APP/PS-1 cerebral cortex arterioles). In these high-power SEMs, roughened irregular contours of capillaries in APP/PS-1 cerebrum are obvious (c) as well as granular distentions of the capillary wall (d).

To deal with this complexity of data, we used MS deconvolution and comparison software linked to multivariate statistical methods to detect metabolites that varied between the feeding regimes (e.g. McDougall et al. 2017). Briefly, all MS data for brain or plasma samples in each ionisation mode were compared by retention time across LCMS runs from all feeding regimes using XCMS software. PCA was used to examine the data and attempt to separate the control fed samples from the raspberry fed samples. For example, the PCA plot (Supplementary Figure S7A) clearly shows that the control feed plasma samples (black symbols) separated from the raspberry feed samples (red and yellow symbols) highlighting that genetic background of the mice

did not influence separation. The OPLS-DA analysis forced separation between the feeding regimes (Supplementary Figure S7B), and examination of the underlying loadings plot (Supplementary Figure S7C) determined metabolites driving this separation as well as metabolites that were significant for the separation of the red and yellow raspberry feed samples from the controls. Using a similar process, OPLS-DA plots were obtained for the plasma samples (+ve mode), and for the brain samples (+ve, -ve mode; Supplementary Figure S8). In all cases, the loadings plots from these OPLS-DA analyses discerned metabolites (i.e.  $m/z$  values) that were driving the separation between the raspberry fed and control feed samples.

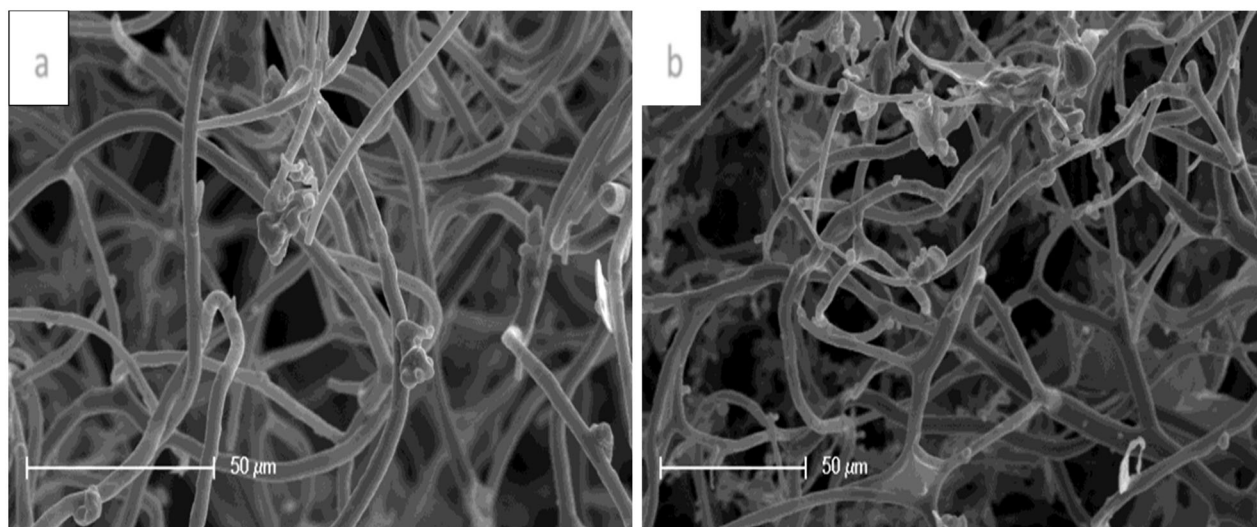


**Figure 5.** SEM images of microvascular corrosion casts from the cerebral microvasculature of an APP/PS-1 transgenic animal supplemented with freeze-dried yellow-raspberry for 6 months. The capillary spacing was irregular and there were conspicuous vessel free areas (a,b). In addition, intertwined and clustered microvessels which is a typical feature of recent sprouting angiogenesis was obvious. Several capillaries had characteristic multi-bulbous microaneurysms (a; arrows) emanating from their lumen. There were also tapered, vessel segments joining capillaries (b) and numerous capillaries with extravasated resin (arrowheads) a feature consistent with polymer leakage from junctions between endothelial cells.

Certain  $m/z$  values were clearly elevated in post raspberry feeding samples. In the plasma samples, four components had increased levels in both the red and yellow raspberry plasma samples (Figure 7), all noted from negative mode data. An early eluting component with an exact  $[M-H]^-$   $m/z$  value of 128.0350 yielded a predicted molecular formula of  $C_5H_7NO_3$ . MS fragmentation data suggested that this was an amino acid derivative and it was putatively identified as pyroglutamate, with levels in the raspberry plasma samples more than double the control samples. Notably two peaks with  $m/z$  128 were noted which could represent two distinct enantiomers. Indeed, a peak with MS properties that match pyroglutamate was also consistently elevated in plasma samples in +ve mode ( $m/z$   $[M+H]^+ = 130.0494$ , predicted formula of  $C_5H_7NO_3$ ). A later eluting compound with an exact  $[M-H]^-$   $m/z$  of 321.0427 yielded a predicted molecular formula of  $C_{15}H_{14}SO_6$ . MS fragmentation data suggested that this was a sulphated metabolite putatively identified as equol sulphate and was  $\sim 9$ -fold higher in the red raspberry plasma samples. A compound with an exact  $m/z$   $[M-H]^-$  value of 580.3251 was  $\sim 3$ -fold higher in the yellow raspberry plasma samples. This had a predicted molecular formula of  $C_{24}H_{48}^{\circ}N_6S$  but yielded no MS<sup>2</sup> fragmentation data and therefore identification is problematic. Finally a compound with an  $m/z$   $[M-H]^-$  value of 215.0816 had 2-fold higher levels in the raspberry plasma samples. This component yielded a predicted molecular formula of  $C_{12}H_{12}^{\circ}N_2$  but gave

uninformative MS fragmentation data. The formula however, suggests it could be an indolyl structure perhaps cyclomethyltryptophan (PubChem 449440) or tetrahydro-carboline-3-carboxylic acid (PubChem 98285).

Using a similar process with the positive mode MS data, other putative metabolites were identified that increased after raspberry feeding in plasma. An increased peak with  $m/z$   $[M+H]^+ = 160.0963$  (predicted formula of  $C_7H_{13}NO_3$ ) was putatively identified as dehydrocarnitine but could be *N*-acetyl-valine or indeed *N*-acetyl-norvaline. MS data from brain samples yielded  $\sim 30$  increased compounds with average abundances  $>2$ -fold greater than control feed levels. However, many of these metabolites gave no useful MS or fragmentation data and their predicted formulae could not be readily tested without further MS analysis. However, there were some plausible hits. A peak with  $m/z$   $[M+H]^+ = 161.1109$  (predicted formula  $C_5H_8N_2O_4$ ) was elevated in the post raspberry feeding brain samples with a putative formula match for thymine glycol. Another peak  $m/z$   $[M+H]^+ = 287.0552$  with a predicted formula of  $C_{15}H_{10}^{\circ}$ , matched some flavonoid components (including kaempferol) but the fragmentation data did not allow conclusive identification.

### **Effects of raspberry consumption behavioural and cognitive functions**

Locomotor activity and anxiety behaviour was measured by OFT in Wild-type and APP/PS-1 genotype



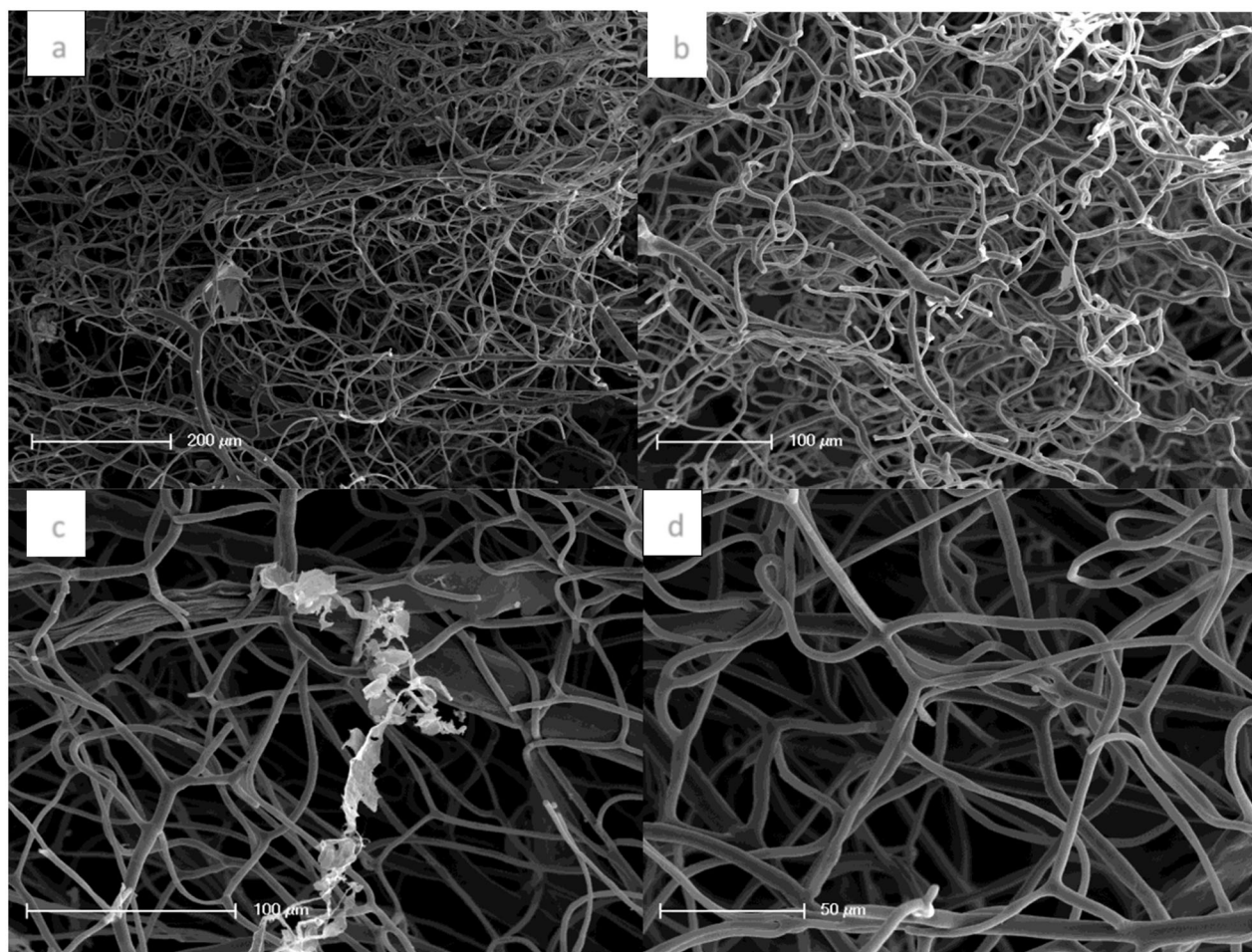


**Figure 6.** SEM of microvascular corrosion casts from the cerebral microvasculature of an APP/PS-1 transgenic animal supplemented with freeze-dried red-raspberry for 6 months. (a) At lower power, the cerebral surface shows the typical capillary clustering around arterioles and venules as well as numerous microvessel free areas. Several clusters of intertwined capillaries were clearly visible (b) and there were numerous blind-ended sprouts suggestive of failed angiogenesis. Microvessel clustering around an arteriole was conspicuous (c). The white flocculent material in (c) is artefactual (remnant) cellular material. Densely packed capillary clusters and narrowed microvessels (top: right of centre in d) characteristic of recent angiogenesis were apparent.

mice, after 6 months consuming red or yellow raspberries. No significant effects of raspberry intake were observed on rearing, grooming, defaecation, linearity, path length or speed when compared with control groups (Supplementary Figure S9). Working memory between wild-type and APP/PS-1 mice was measured using the two-stage test (acquisition and test). There were no significant differences observed in either acquisition or test phase in 10-month-old wild-type mice compared with APP/PS-1 mice nor in response to dietary regimes (Supplementary Figure S10).

With respect to spatial learning in the MWM (Figure 8a), wild-type mice on the control diet for 24 weeks showed no significant changes in escape latency, path length or speed. Escape latency remained non-significant on the remaining days. There were no statistically significant differences in either path length or speed among groups fed the control diet or

treatments for 24 weeks. As an indication of memory retention, the probe trial (Figure 8b) demonstrated that quadrant times were similar between control-, red raspberry- and yellow raspberry-fed mice in both wild-type and APP/PS-1 mice. Results failed to reach significance  $p < 0.05$ . Within the APP/PS-1 group, although there was a trend towards increased time spent in the target quadrant, this failed to reach significance.

#### **Impact of raspberry feeding on faecal microbiota composition**

The effects of red and yellow raspberry intake on the gut microbiota of wild-type and transgenic mice were profiled using 16S rRNA Illumina sequencing technology. Bacterial richness within each sample did not change significantly (Figure 9a). Bray-Curtis dissimilarity index, measuring within and between group



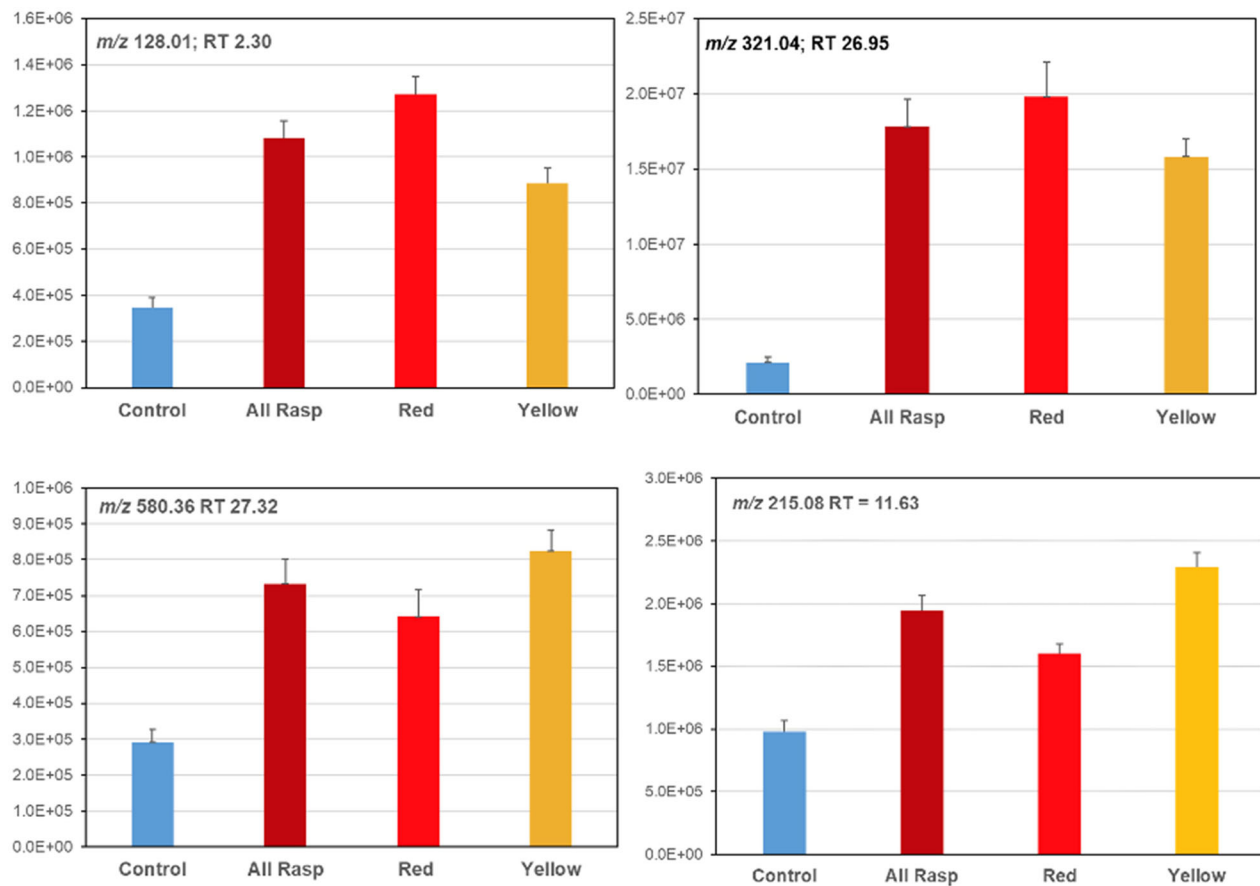


**Figure 7.** Relative abundance of *m/z* values elevated in post raspberry feeding plasma samples.

dissimilarities showed differences depending on mouse genotype. Specifically, in the APP-PS1 mice, ingestion of both red and yellow raspberries increased community dissimilarity compared with the control diet, with red raspberry having a greater effect. This was not observed in the wild-type animals (Figure 9b).

We compared the relative abundances between the three different dietary regimes for each mouse genetic background at different taxonomic levels focussing on dominant and prevalent taxa only (excluding low abundant taxa < 0.01 percent relative abundance and excluding rare taxa present in less than 25% of samples). Some changes in the relative abundance at phylum level were observed (Figure 9c and Table 2). In particular yellow raspberry intake induced a decrease in Bacteroidetes ( $92.680 \pm 3.05$ ) with respect to control diet in wild-type mice ( $98.077 \pm 0.66$ , FDR correct  $p = 0.0303$ ), while an increase in Proteobacteria was also observed [yellow raspberry fed ( $2.225 \pm 1.05$ ) vs. control diet fed wild-type mice ( $0.450 \pm 0.26$ ), FDR corrected  $p = 0.0303$ ].

## Discussion

Globally, populations are ageing giving rise to increased cognitive impairment and burden including rising

levels of AD. Lack of effective treatments makes it essential to consider approaches and strategies for prolonging healthy cognitive ageing. Evidence suggests that the traditional Mediterranean diet, which is rich in fibre and polyphenols can help prevent or delay cognitive dysfunction in the elderly, and preserve healthy brain structure and function (Shishtar et al. 2020). Polyphenols are likely to be important mediators as flavanols and anthocyanins have been associated with lower AD risk (Shishtar et al. 2020). Disruption of microvascular architecture is common in the early pathogenesis of AD and is gaining prominence as a potential therapeutic target.

The functional unit of the circulatory system is the microvasculature comprising capillaries, venules and arterioles whose internal diameter (in mice) is generally less than  $10 \mu\text{m}$  (Farkas and Luiten 2001). Gaseous transfer, particularly  $\text{O}_2$  and  $\text{CO}_2$ , in addition to nutrients and metabolites are exchanged across the endothelial membranes and the intervening tissues (such as the thin alveolar epithelium in the lung) making the microvasculature the primary organ responsible for mediating tissue and organ homeostasis. Capillaries, in the majority of tissues, are generally less than  $50 \mu\text{m}$  apart (reflecting the optimal diffusion

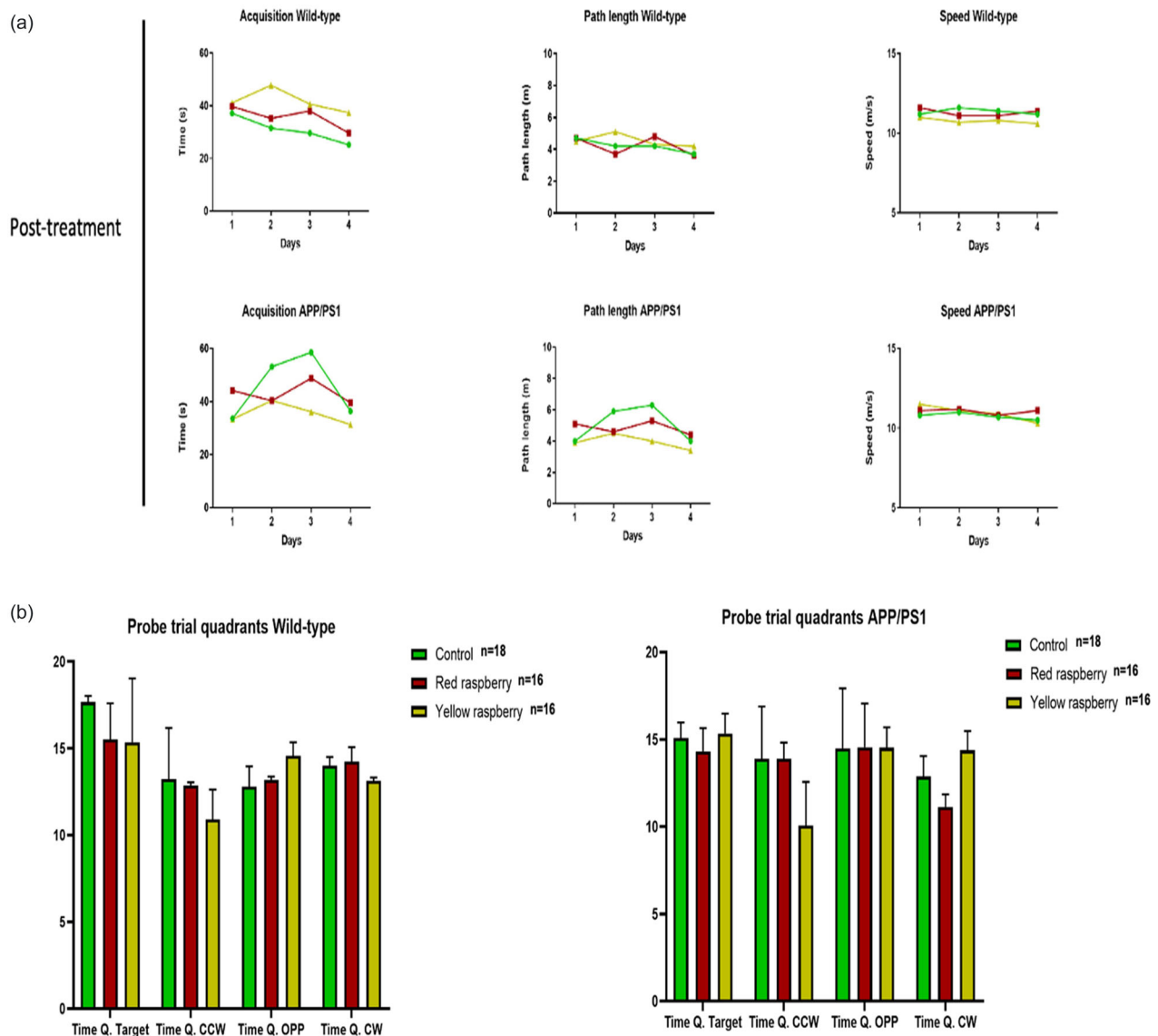


**Figure 8.** Effects of raspberry supplementation on cognitive performance in wild-type and APP/PS1 mice in the Morris water maze with respect to (a) escape latency, path length and speed of wild-type and APP/PS1 mice. (b) Memory recall assessed as time spent in the each quadrant (Q) of the Morris water maze for both wild-type and APP/PS-1 mice. Target quadrant (Q target), quadrant opposite target Q (Q. Opp), quadrant clockwise Oom target Q (Q.CW), quadrant counterclockwise Oom target Q (Q.CCW). Data represent mean  $\pm$  SEM.

distance of  $O_2$ ) and are the dominant class of microvessels. Microvascular patency and optimisation of flow through capillary plexi, is thus critical for regulation of tissue hypoxia and maintenance of function. There is a reciprocal dependency between the tissue stroma and the supplying microvasculature: loss of microvessels leads to tissue death (such as in thrombosis or stroke) and change in tissue volume that accompanies cortical atrophy during the course of AD is reflected in a local change in microvessel density. In this study, we employed microvascular corrosion casting, a technique which produces exquisite ultrastructural detail and faithful replication of the luminal surface of the microvasculature within the cerebral

hemispheres of APP/PS-1 transgenic mice or their wild-type C57Bl/6J littermates (Ackermann and Konerding 2015). We used this technique to test the hypothesis that 6 months of dietary supplementation with yellow or red berries (with low and high polyphenol content, respectively) can rescue these microvascular pathologies in APP/PS-1 transgenic mice. Previously, our group has shown that cerebral microvascular alterations in APP/PS-1 mice at 3–4 months of age include clusters of intertwined microvessels (characteristic of recent angiogenesis), signs of inter-endothelial leakage, microaneurisms, variations in individual capillary diameters and bulbous extensions to the endothelial luminal wall (Kelly et al. 2017). The

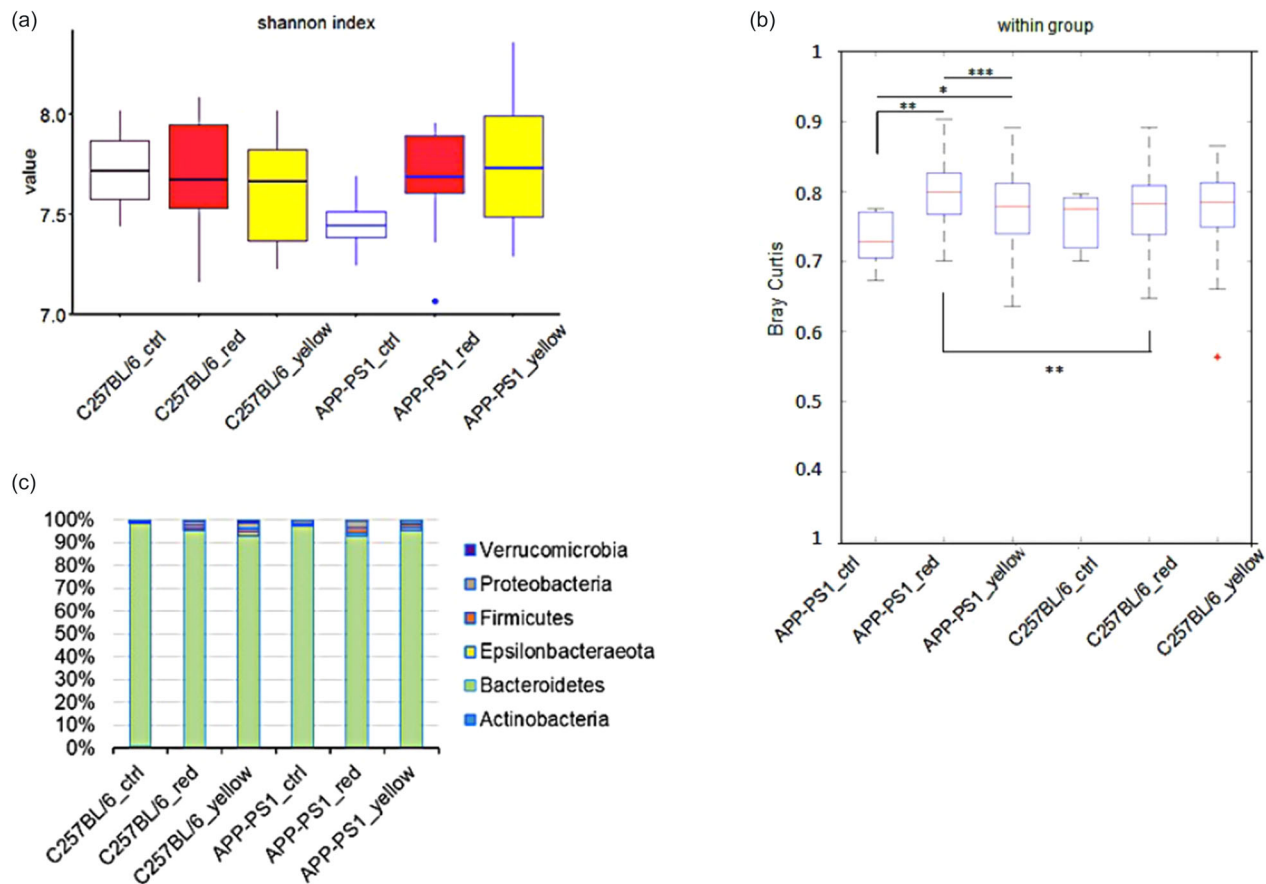


**Figure 9.** Measure of bacterial diversity. (a) Alpha-diversity calculated with the Shannon entropy index. No statistically significant differences were detected. The body of the box plot represents the first and third quartiles of the distribution, and the median. The whiskers extend from the quartiles to the last data-point within  $1.5 \times$  IQR, with outliers beyond represented as dots. (b) Measure of beta diversity based on the Bray-Curtis dissimilarity index according to groups of treatments. Within group versus between group dissimilarity. \* $p < 0.05$ , \*\* $p < 0.01$  and \*\*\* $p < 0.001$ , Wilcoxon sum rank test. (c) Relative abundance of microbial taxa at phylum level.

**Table 2.** Relative abundance at a phylum level.

Phyla	WT Control	WT Red	WT Yellow	APP/PS1 Control	APP/PS1 Red	APP/PS1 Yellow
Actinobacteria	0.51 (0.3)	0.19 (0.29)	0.42 (0.45)	0.05 (0.10)	0.18 (0.26)	0.41 (0.69)
Bacteroidetes	98.08 (0.66)*	95.23 (2.22)	92.68 (3.05)*	97.05 (0.19)	92.72 (4.70)	94.84 (4.05)
Epsilonbacteraeota	0.48 (0.47)	0.59 (0.64)	1.31 (1.96)	0.138 (0.19)	1.13 (0.75)	1.27 (1.62)
Firmicutes	0.49 (0.18)	1.75 (1.29)	1.75 (0.98)	0.84 (0.70)	2.53 (3.65)	1.35 (1.31)
Proteobacteria	0.45 (0.26)*	1.64 (1.64)	2.23 (1.05)*	1.46 (1.17)	2.89 (1.65)	1.70 (1.30)
Verrucomicrobia	0.00 (0.00)	0.60 (1.17)	1.62 (2.52)	0.47 (0.60)	0.565 (1.2)	0.43 (1.00)

Data are reported as percentage, mean ( $\pm$ SD) of the relative abundance of microbial taxa at the phylum level, for each condition. Yellow raspberry fed wild-type (WT) shows a significant decrease in Bacteroidetes and increase in Proteobacteria, compared with control diet (Wilcoxon sum rank test at \* $p < 0.05$ , in bold).

cerebral microvascular alterations observed in 3–4-month-old APP/PS-1 transgenic mice precede cognitive decline that is characteristic in these mice. Severe microvessel pathologies in 10–11-month-old mice coincide with the onset of cognitive decline and 100–200  $\mu$ m diameter holes in the cortical vasculature, that give the gross architecture a ‘moth-eaten’ appearance (Kelly et al. 2015), similar to those observed in the murine APP23 model (Meyer et al. 2008). Cerebral hypoperfusion at 2–3 months of age,

is also an early sign of perturbed microvascular structure in the Tg2576 murine model of AD, occurring significantly earlier than the decline in cognitive performance at 11–13 months (Niwa et al. 2002). In the present study, the changes in microvascular morphology we previously described (Kelly et al. 2015, 2017) were similarly observed in cerebral microvasculature of 10-month-old APP/PS-1 transgenic mice when compared with littermate controls. Careful ultrastructural examination of cerebral microvascular morphology in



treated (either yellow or red raspberry) compared with control diet revealed that the range of pathologies observed was unaffected following 6 months of dietary supplementation with berries in APP/PS-1 transgenic mice. Temporal progression of microvascular pathology is a consistent observation in all of the murine models of AD, with the majority of these changes detected at 3–9 months (reviewed by Szu and Obenaus 2021), prior to the onset of cognitive decline. Similarly, human AD is characterised by gross perturbations in cerebro-vascular flow and post-mortem macro and microvascular changes that have led to a ‘two-hit’ vascular hypothesis involving A $\beta$  deposition in the brain. The first ‘hit’ is considered to be vascular damage as a result of perivascular amyloid deposition, that results in an increase in A $\beta$  accumulation in the brain parenchyma or ‘hit 2’. Macrovascular perfusion abnormalities, microvascular pathology and BBB breakdown has also been observed in patients with mild cognitive impairment who were stratified for levels of circulating A $\beta$  consistent with the hypothesis that this phenomenon is an early marker of AD (Nation et al. 2019). Although our intervention with berries did not lead to a reduction in vascular pathology in the APP/PS-1 mice, lifestyle factors are long known to be associated with an increased risk of AD. In particular, the effect of reduced levels of exercise, poor diet and adverse gut microbiota on brain microvascular health is under-represented in the literature making this an attractive area for future research.

Consumption of red and yellow freeze-dried raspberries produced consistent changes in putative endogenous metabolites in both the brain and plasma of wild-type and APP/PS-1 mice. However, as our method did not employ solid phase extraction (SPE) methods to specifically enrich potential polyphenol metabolites (Kay et al. 2004), they were effectively swamped by other more abundant endogenous components and their relatively low abundance meant that they were not available for MS<sup>2</sup> fragmentation. However, the lack of SPE avoided restriction of the types of metabolites that could be identified in the samples. Indeed, components putatively identified as enriched in post raspberry feeding plasma samples included amino acids derivatives such as pyroglutamate, cyclomethyl tryptophan and potential carnitine metabolites. Interestingly, pyroglutamate containing A $\beta$  have been found to be increased during AD (Jawhar et al. 2011) but increased serum levels of pyroglutamate have not been reported. Dehydrocarnitine has been suggested to be a biomarker for early onset AD (Liang et al. 2015; Lee et al. 2016) However, as no confirmatory MS<sup>2</sup> information was obtained, other matches

include *N*-acetyl-valine or *N*-acetyl-norvaline which has been identified in cultured astrocytes (Kiray 2015). Another candidate component had  $m/z$   $[M+H]^+ = 302.2317$  which gave a predicted formula of C<sub>16</sub>H<sub>31</sub>NO<sub>4</sub>, but no MS<sup>2</sup> data were available. However, a match to this formula was noted in a study of human plasma metabolites associated with AD and identified as nonanoyl carnitine or dimethylheptanoyl carnitine (Vardarajan et al. 2020). Potential metabolites enriched in +raspberry brain samples included thymine glycol, an altered base that may arise from oxidative damage of DNA in Alzheimer’s (Lyras et al. 1997), and known to be produced in mice (Adelman et al. 1988). The identification of a potential isomer of kaempferol is of interest as a similar component has been noted in studies of phenolic derivatives in brain samples and may be an isomer of kaempferol with different hydroxylation pattern (personal communication; CD Kay). Equol sulphate was also identified as potentially increased in +raspberry plasma and it has been shown that raspberry intake can alter mouse microbiota to produce higher levels of equol (Xian et al. 2021), which could be metabolised and circulated as equol sulphate in the plasma.

An altered gut microbiota in AD is well documented and is now thought to play an important role to play in regulating systemic and neuroinflammation which drives A $\beta$  plaque formation (Rutsch et al. 2020). The gut microbiota and their metabolites, specifically the short chain fatty acids (acetate, propionate and butyrate), and small phenolic acids derived from microbial metabolism of complex plant polyphenols play a regulatory role in both the intestinal barrier and the BBB (Hoyle et al. 2018; Ghosh et al. 2021). In the current study, we show that raspberry ingestion can modulate the gut microbiota with greatest effect seen in the APP-PS1 mice compared with the wild-type background strain (C57Bl/6J mice). Although microbiota modulation by the powder raspberries was modest, the fact that it was statistically significant indicates a potential to act on AD associated microbiota dysbiosis in terms of  $\beta$ -diversity (Bray-Curtis dissimilarity index). Previous studies in pre-clinical models have demonstrated microbiota modulators include probiotic bacteria (Wang et al. 2020; Zhu et al. 2021) human commensal bacteria (Ou et al. 2020), butyrate producing bacteria (Sun et al. 2020; Go et al. 2021), prebiotics (Sun et al. 2019; Han et al. 2020; Lee et al. 2021) and polyphenols. These can improve barrier function, reduce neuroinflammation and limit A $\beta$  plaque formation in the hippocampus, improving cognitive function in model systems (Wang et al. 2021).

A limitation of the current work is the unequal number of animals on control diet or diet supplemented with raspberry, which could have impacted on our ability to discern statistically significant differences between control and raspberry fed animals.

From a cognitive perspective, the long-term feeding of male C57Bl/6J & APP/PS-1 mice with the freeze dried anthocyanin-rich (red) or -poor (yellow) *R. idaeus* berries (100 mg/day) mice elicited few changes in behaviour at ~10 months old. This contrasts with neuroprotective effects observed in other studies using the APP/PS1 transgenic models and polyphenol extracts, albeit with older mice (i.e. 13–15 months). For example, an ethanol extract of mulberry fruit (100 mg/kg body weight, for 1.5–3 weeks) improved the spatial memory and learning ability of APP/PS1 mice (Liu and Du 2020). While APP/PS1 mice fed chow enriched in commercial anthocyanin-rich bilberry (1.53 mg/g) or blackcurrant (1.43 mg/g) extracts for ~10 months alleviated spatial working memory deficit (MWM) of the aged mice (13 months) compared with control diet (Vepsäläinen et al. 2013). Also, a blueberry extract fed to aged APP/PS1 mice for 16 weeks (Tan et al. 2017) and a polyphenolic-enriched extract from blueberries and grapes (500 or 2500 mg/kg body weight) fed to aged triple-transgenic APP/PS1/Tau mice for 4 months which resulted in significant improvements in object recognition in mice aged ~15 months versus control (Dal-Pan et al. 2016). It is possible that differences between the polyphenol composition of the fruits used influenced the lack of effect as raspberries are generally lower in anthocyanins and contain considerable amounts of ellagitannins and ellagic acid constituents (Table 1; McDougall et al. 2017) compared with the berries discussed above. However, a more feasible reason for our lack of neuroprotective effects may be matrix and dosage, in that the previous studies used commercial or in-house polyphenolic-enriched extracts of various berries, whereas this study used powdered whole berries. These semi-purified polyphenol extracts contain much higher levels of polyphenols than whole fruit powders and they lack the soluble and insoluble fibre present in whole fruits. In our study, the total polyphenol dose per day from the powdered raspberries was 0.27 mg (yellow) or 3.26 mg (red) which contrasts that of Dal-Pan et al. (2016) where mice consumed ~10 mg or 50 mg of polyphenolic-enriched extract per day (i.e. doses of 500 or 2500 mg/kg body weight assuming an average mouse weight of 20 g) or the ethanolic mulberry extract were mice were dosed at ~2 mg p.d. Liu and Du (2020). However, comparison

of actual polyphenol doses is difficult because the extraction and removal of the berry pulp could easily increase the polyphenol content of such enriched extracts by 20–50-fold over the original fruits. Our strategy was to use an achievable diet based whole raspberry intervention rather than using polyphenol extracts that would deliver daily supraphysiologically-relevant amounts of polyphenols. A final consideration is the age of the mice, cognitive function was a primary endpoint in the above studies and consequently the mice were older (aged between 13 and 15 months) to ensure a significant cognitive deficit would be evident. In this study however, the mice were ~10 months old at conclusion of the study because we were focussed on detecting early changes in the cerebral microvascular of the APP/PS1 vs. C57Bl/6J wild type.

## Conclusion

The APP/PS1 mice evidenced dysregulated microvasculature consistent with earlier studies by our group (Kelly et al. 2015, 2017). However, in contrast to the use of the diabetic drug Liraglutide, the feeding of *R. idaeus* berries at levels consistent with average human intake, did not restore microvascular architecture to that observed in wild-type, age-matched littermates. Raspberry feeding did modulate endogenous metabolites present in the brain/plasma of the mice, as well as gut microbiota in AD vs. wild-type albeit to a modest extent indicating some potential to act on AD-associated microbiota dysbiosis.

## Acknowledgements

We acknowledge funding from the National Processed Raspberry Council who had no involvement in study design; in the collection, analysis and interpretation of data; in the writing of the report and in the decision to submit the article for publication.

## Disclosure statement

No potential conflict of interest was reported by the authors.

## Funding

This work was supported by the National Processed Raspberry Council (201881).

## ORCID

L. Kirsty Pourshahidi  <http://orcid.org/0000-0003-2251-5251>  
 William Allwood  <http://orcid.org/0000-0001-6433-2694>  
 Gordon McDougall  <http://orcid.org/0000-0002-2285-0124>  
 Chris I. R. Gill  <http://orcid.org/0000-0003-4335-7571>

## References

- Ackermann M, Konerding M. 2015. Vascular casting for the study of vascular morphogenesis. *Methods Mol Biol* (Clifton, N.J.). 1214:49–66.
- Adelman R, Saul RL, Ames BN. 1988. Oxidative damage to DNA: relation to species metabolic rate and life span. *Proc Natl Acad Sci USA*. 85(8):2706–2708.
- Allwood JW, Weber RJM, Zhou J, He S, Viant MR, Dunn WB. 2013. CASMI—the small molecule identification process from a Birmingham perspective. *Metabolites*. 3(2):397–411.
- Beckmann N, Schuler A, Mueggler T, Meyer E, Wiederhold K, Staufenbiel M, Krucker T. 2003. Age-dependent cerebrovascular abnormalities and blood flow disturbances in APP23 mice modeling Alzheimer's disease. *J Neurosci*. 23(24):8453–8459.
- Benjamini Y, Hochberg Y. 1995. Controlling the false discovery rate: a practical and powerful approach to multiple testing. *J Royal Stat Soc Series B (Methodological)*. 57(1):289–300.
- Berendsen AM, Kang JH, Feskens EJM, de Groot CPGM, Grodstein F, van de Rest O. 2018. Association of long-term adherence to the MIND Diet with cognitive function and cognitive decline in American women. *J Nutr Health Aging*. 22(2):222–229.
- Bookheimer SY, Strojwas MH, Cohen MS, Saunders AM, Pericak-Vance MA, Mazziotta JC, Small GW. 2000. Patterns of brain activation in people at risk for Alzheimer's disease. *N Engl J Med*. 343(7):450–456.
- Brown M, Wedge DC, Goodacre R, Kell DB, Baker PN, Kenny LC, Mamas MA, Neyses L, Dunn WB. 2011. Automated workflows for accurate mass-based putative metabolite identification in LC/MS-derived metabolomic datasets. *Bioinformatics*. 27(8):1108–1112.
- Callahan BJ, McMurdie PJ, Rosen MJ, Han AW, Johnson AJA, Holmes SP. 2016. DADA2: high-resolution sample inference from Illumina amplicon data. *Nat Methods*. 13(7):581–583.
- Cao J, Amakye WK, Qi C, Liu X, Ma J, Ren J. 2021. *Bifidobacterium Lactis* Probio-M8 regulates gut microbiota to alleviate Alzheimer's disease in the APP/PS1 mouse model. *Eur J Nutr*. 60(7):3757–3769.
- Caporaso JG, Kuczynski J, Stombaugh J, Bittinger K, Bushman FD, Costello EK, Fierer N, Peña AG, Goodrich JK, Gordon JI, et al. 2010. QIIME allows analysis of high-throughput community sequencing data. *Nat Methods*. 7(5):335–336.
- Dal-Pan A, Dudonné S, Bourassa P, Bourdoulous M, Tremblay C, Desjardins Y, Calon F, on behalf of the Neurophenols consortium 2016. Cognitive-enhancing effects of a polyphenols-rich extract from fruits without changes in neuropathology in an animal model of Alzheimer's disease. *JAD*. 55(1):115–135.
- El Gaamouch F, Liu K, Lin H, Wu C, Wang J. 2021. Development of grape polyphenols as multi-targeting strategies for Alzheimer's disease. *Neurochem Int*. 147:105046.
- Elmaleh DR, Downey MA, Kundakovic L, Wilkinson JE, Neeman Z, Segal E. 2021. New approaches to profile the microbiome for treatment of neurodegenerative disease. *J Alzheimers Dis*. 82(4):1373–1401.
- Fan X, Liu B, Zhou J, Gu X, Zhou Y, Yang Y, Guo F, Wei X, Wang H, Si N, et al. 2021. High-fat diet alleviates neuroinflammation and metabolic disorders of APP/PS1 mice and the intervention with chinese medicine. *Front Aging Neurosci*. 13:658376.
- Farkas E, Luiten PGM. 2001. Cerebral microvascular pathology in aging and Alzheimer's disease. *Prog Neurobiol*. 64(6):575–611.
- Ghosh S, Whitley CS, Haribabu B, Jala VR. 2021. Regulation of intestinal barrier function by microbial metabolites. *Cell Mol Gastroenterol Hepatol*. 11(5):1463–1482.
- Gildawie KR, Galli RL, Shukitt-Hale B, Carey AN. 2018. Protective effects of foods containing flavonoids on age-related cognitive decline. *Curr Nutr Rep*. 7(2):39–48.
- Go J, Chang D, Ryu Y, Park H, Lee I, Noh J, Hwang DY, Kim B, Kim K, Lee C. 2021. Human gut microbiota *Agathobaculum butyriciproducens* improves cognitive impairment in LPS-induced and APP/PS1 mouse models of Alzheimer's disease. *Nutr Res*. 86:96–108.
- Han D, Li Z, Liu T, Yang N, Li Y, He J, Qian M, Kuang Z, Zhang W, Ni C, et al. 2020. Prebiotics regulation of intestinal microbiota attenuates cognitive dysfunction induced by surgery stimulation in APP/PS1 mice. *Aging Dis*. 11(5):1029–1045.
- Hendrickx JO, Martinet W, Van Dam D, De Meyer , Guido RY. 2021. Inflammation, nitro-oxidative stress, impaired autophagy, and insulin resistance as a mechanistic convergence between arterial stiffness and Alzheimer's disease. *Front Mol Biosci*. 8:651215.
- Herring WL, Gould IG, Fillit H, Lindgren P, Forrestal F, Thompson R, Pemberton-Ross P. 2021. Predicted lifetime health outcomes for aducanumab in patients with early Alzheimer's disease. *Neurol Ther*. 10(2):919–940.
- Hoyle L, Snelling T, Umlai U, Nicholson JK, Carding SR, Glen RC, McArthur S. 2018. Microbiome-host systems interactions: protective effects of propionate upon the blood-brain barrier. *Microbiome*. 6(1):55.
- Jawhar S, Wirths O, Bayer TA. 2011. Pyroglutamate amyloid- $\beta$  (A $\beta$ ): a hatchet man in Alzheimer disease. *J Biol Chem*. 286(45):38825–38832.
- Jefferies WA, Price KA, Biron KE, Fenninger F, Pfeifer CG, Dickstein DL. 2013. Adjusting the compass: new insights into the role of angiogenesis in Alzheimer's disease. *Alzheimers Res Ther*. 5(6):64.
- Joshua M, Okere C, Sylvester OP, Yahaya M, Precious O, Dluya T, Um J, Neksumi M, Boyd J, Vincent-Tyndall J, et al. 2017. Disruption of angiogenesis by anthocyanin-rich extracts of *Hibiscus sabdariffa*. *Int J Sci Eng Res*. 8(2):299–307.



- Kay CD, Mazza G, Holub BJ, Wang J. 2004. Anthocyanin metabolites in human urine and serum. *Br J Nutr.* 91(6): 933–942.
- Kelly P, Denver P, Satchell SC, Ackermann M, Konerding MA, Mitchell CA. 2017. Microvascular ultrastructural changes precede cognitive impairment in the murine APP<sup>swe</sup>/PS1<sup>dE9</sup> model of Alzheimer's disease. *Angiogenesis.* 20(4):567–580.
- Kelly P, McClean PL, Ackermann M, Konerding MA, Hölscher C, Mitchell CA. 2015. Restoration of cerebral and systemic microvascular architecture in APP/PS1 transgenic mice following treatment with Liraglutide<sup>TM</sup>. *Microcirculation.* 22(2):133–145.
- Khan A, Kalaria RN, Corbett A, Ballard C. 2016. Update on vascular dementia. *J Geriatr Psychiatry Neurol.* 29(5): 281–301.
- Kiray H. 2015. Identification of astrocytic factors that could play a role in myelination. University of Glasgow. <https://eleanor.lib.gla.ac.uk/record=b3120656>.
- Klindworth A, Pruesse E, Schweer T, Peplies J, Quast C, Horn M, Glöckner FO. 2013. Evaluation of general 16S ribosomal RNA gene PCR primers for classical and next-generation sequencing-based diversity studies. *Nucleic Acids Res.* 41(1):e1.
- Knopman DS, Roberts R. 2010. Vascular risk factors: imaging and neuropathologic correlates. *J Alzheimers Dis.* 20(3):699–709.
- Lamar M, Boots EA, Arfanakis K, Barnes LL, Schneider JA. 2020. Common brain structural alterations associated with cardiovascular disease risk factors and Alzheimer's dementia: future directions and implications. *Neuropsychol Rev.* 30(4):546–557.
- Lamport DJ, Williams CM. 2021. Polyphenols and cognition in humans: an overview of current evidence from recent systematic reviews and meta-analyses. *Brain Plast.* 6(2): 139–153.
- Lee J, Choi J, Wong GW, Wolfgang MJ. 2016. Neurometabolic roles of ApoE and Ldl-R in mouse brain. *J Bioenerg Biomembr.* 48(1):13–21.
- Lee Y, Lai D, Huang H, Lee-Chen G, Chang C, Hsieh-Li HM, Lee G. 2021. Prebiotic lactulose ameliorates the cognitive deficit in Alzheimer's disease mouse model through macroautophagy and chaperone-mediated autophagy pathways. *J Agric Food Chem.* 69(8): 2422–2437.
- Liang Q, Liu H, Zhang T, Jiang Y, Xing H, Zhang A. 2015. Metabolomics-based screening of salivary biomarkers for early diagnosis of Alzheimer's disease. *RSC Adv.* 5(116): 96074–96079.
- Liu D, Du D. 2020. Mulberry fruit extract alleviates cognitive impairment by promoting the clearance of amyloid- $\beta$  and inhibiting neuroinflammation in Alzheimer's disease mice. *Neurochem Res.* 45(9):2009–2019.
- Lyras L, Cairns NJ, Jenner A, Jenner P, Halliwell B. 1997. An assessment of oxidative damage to proteins, lipids, and DNA in brain from patients with Alzheimer's disease. *J Neurochem.* 68(5):2061–2069.
- McDougall GJ, Allwood JW, Pereira-Caro G, Brown EM, Verrall S, Stewart D, Latimer C, McMullan G, Lawther R, O'Connor G, et al. 2017. Novel colon-available triterpenoids identified in raspberry fruits exhibit antigenotoxic activities in vitro. *Mol Nutr Food Res.* 61(2):1600327.
- Meyer EP, Ulmann-Schuler A, Staufenbiel M, Krucker T. 2008. Altered morphology and 3D architecture of brain vasculature in a mouse model for Alzheimer's disease. *Proc Natl Acad Sci U S A.* 105(9):3587–3592.
- Miller MG, Hamilton DA, Joseph JA, Shukitt-Hale B. 2018. Dietary blueberry improves cognition among older adults in a randomized, double-blind, placebo-controlled trial. *Eur J Nutr.* 57(3):1169–1180.
- Morris MC, Tangney CC, Wang Y, Sacks FM, Barnes LL, Bennett DA, Aggarwal NT. 2015. MIND diet slows cognitive decline with aging. *Alzheimers Dement.* 11(9): 1015–1022.
- Nation DA, Sweeney MD, Montagne A, Sagare AP, D'Orazio LM, Pachicano M, Sepeshband F, Nelson AR, Buennagel DP, Harrington MG, et al. 2019. Blood-brain barrier breakdown is an early biomarker of human cognitive dysfunction. *Nat Med.* 25(2):270–276.
- Niwa K, Kazama K, Younkin SG, Carlson GA, Iadecola C. 2002. Alterations in cerebral blood flow and glucose utilisation in mice overexpressing the amyloid precursor protein. *Neurobiol Dis.* 9(1):61–68.
- Ou Z, Deng L, Lu Z, Wu F, Liu W, Huang D, Peng Y. 2020. Protective effects of Akkermansia muciniphila on cognitive deficits and amyloid pathology in a mouse model of Alzheimer's disease. *Nutr Diabetes.* 10(1):12.
- Pfeifer LA, White LR, Ross GW, Petrovitch H, Launer LJ. 2002. Cerebral amyloid angiopathy and cognitive function: the HAAS autopsy study. *Neurology.* 58(11): 1629–1634.
- Quast C, Pruesse E, Yilmaz P, Gerken J, Schweer T, Yarza P, Peplies J, Glöckner FO. 2013. The SILVA ribosomal RNA gene database project: improved data processing and web-based tools. *Nucleic Acids Res.* 41(Database issue), 590.
- Román GC, Jackson RE, Gadhia R, Román AN, Reis J. 2019. Mediterranean diet: the role of long-chain  $\omega$ -3 fatty acids in fish; polyphenols in fruits, vegetables, cereals, coffee, tea, cacao and wine; probiotics and vitamins in prevention of stroke, age-related cognitive decline, and Alzheimer disease. *Rev Neurol (Paris).* 175(10):724–741.
- Rutledge GA, Sandhu AK, Miller MG, Edirisinghe I, Burton-Freeman BB, Shukitt-Hale B. 2021. Blueberry phenolics are associated with cognitive enhancement in supplemented healthy older adults. *Food Funct.* 12(1): 107–118.
- Rutsch A, Kantsjö JB, Ronchi F. 2020. The gut-brain axis: how microbiota and host inflammasome influence brain physiology and pathology. *Front Immunol.* 11:604179.
- Saito S, Yamamoto Y, Maki T, Hattori Y, Ito H, Mizuno K, Harada-Shiba M, Kalaria RN, Fukushima M, Takahashi R, et al. 2017. Taxifolin inhibits amyloid- $\beta$  oligomer formation and fully restores vascular integrity and memory in cerebral amyloid angiopathy. *Acta Neuropathol Commun.* 5(1):26.
- Serrano-Pozo A, Frosch MP, Masliah E, Hyman BT. 2011. Neuropathological alterations in Alzheimer disease. *Cold Spring Harb Perspect Med.* 1(1):a006189.
- Shishtar E, Rogers GT, Blumberg JB, Au R, Jacques PF. 2020. Long-term dietary flavonoid intake and risk of Alzheimer disease and related dementias in the Framingham Offspring Cohort. *Am J Clin Nutr.* 112(2): 343–353.

- Srivastava S, Ahmad R, Khare SK. 2021. Alzheimer's disease and its treatment by different approaches: a review. *Eur J Med Chem.* 216:113320.
- Steinman J, Sun H, Feng Z. 2020. Microvascular alterations in Alzheimer's Disease. *Front Cell Neurosci.* 14:618986.
- Sun J, Liu S, Ling Z, Wang F, Ling Y, Gong T, Fang N, Ye S, Si J, Liu J. 2019. Fructooligosaccharides ameliorating cognitive deficits and neurodegeneration in APP/PS1 transgenic mice through modulating gut microbiota. *J Agric Food Chem.* 67(10):3006–3017.
- Sun J, Xu J, Yang B, Chen K, Kong Y, Fang N, Gong T, Wang F, Ling Z, Liu J. 2020. Effect of *Clostridium butyricum* against microglia-mediated neuroinflammation in Alzheimer's disease via regulating gut microbiota and metabolites butyrate. *Mol Nutr Food Res.* 64(2):e1900636.
- Szu JI, Obenaus A. 2021. Cerebrovascular phenotypes in mouse models of Alzheimer's disease. *J Cereb Blood Flow Metab.* 41(8):1821–1841.
- Tan L, Yang H, Pang W, Li H, Liu W, Sun S, Song N, Zhang W, Jiang Y. 2017. Investigation on the role of BDNF in the benefits of blueberry extracts for the improvement of learning and memory in Alzheimer's disease mouse model. *J Alzheimers Dis.* 56(2):629–640.
- Tsakiroglou P, VandenAkker NE, Bo' CD, Riso P, Klimis-Zacas D. 2019. Role of berry anthocyanins and phenolic acids on cell migration and angiogenesis: an updated overview. *Nutrients.* 11(5):1075.
- Vardarajan B, Kalia V, Manly J, Brickman A, Reyes Dumeyer D, Lantigua R, Ionita Laza I, Jones DP, Miller GW, Mayeux R, et al. 2020. Differences in plasma metabolites related to Alzheimer's disease, APOE  $\epsilon$ 4 status, and ethnicity. *Alzheimer's & Dementia.* *Alzheimers Dement (NY).* 6(1):e12025.
- Vepsäläinen S, Koivisto H, Pekkarinen E, Mäkinen P, Dobson G, McDougall GJ, Stewart D, Haapasalo A, Karjalainen RO, Tanila H, et al. 2013. Anthocyanin-enriched bilberry and blackcurrant extracts modulate amyloid precursor protein processing and alleviate behavioral abnormalities in the APP/PS1 mouse model of Alzheimer's disease. *J Nutr Biochem.* 24(1):360–370.
- Wang Y, Lim Y, He Z, Wong W, Lai W. 2021. Dietary phytochemicals that influence gut microbiota: roles and actions as anti-Alzheimer agents. *Crit Rev Food Sci Nutr.* 62(19):1–27.
- Wang F, Xu T, Zhang Y, Zheng T, He Y, He F, Jiang Y. 2020. Long-term combined administration of *Bifidobacterium bifidum* TMC3115 and *Lactobacillus plantarum* 45 alleviates spatial memory impairment and gut dysbiosis in APP/PS1 mice. *FEMS Microbiology Letters.* 367(7):fnaa048.
- Wimo A, Guerchet M, Ali G, Wu Y, Prina AM, Winblad B, Jönsson L, Liu Z, Prince M. 2017. The worldwide costs of dementia 2015 and comparisons with 2010. *Alzheimers Dement.* 13(1):1–7.
- Wu Q, Li Q, Zhang X, Ntim M, Wu X, Li M, Wang L, Zhao J, Li S. 2020. Treatment with *Bifidobacteria* can suppress A $\beta$  accumulation and neuroinflammation in APP/PS1 mice. *PeerJ.* 8:e10262.
- Xian Y, Fan R, Shao J, Mulcahy Toney A, Chung S, Ramer-Tait AE. 2021. Polyphenolic fractions isolated from red raspberry whole fruit, pulp, and seed differentially alter the gut microbiota of mice with diet-induced obesity. *J Funct Foods.* 76:104288.
- Zhu G, Zhao J, Zhang H, Chen W, Wang G. 2021. Administration of *Bifidobacterium breve* improves the brain function of A $\beta$ 1-42-treated mice via the modulation of the gut microbiome. *Nutrients.* 13(5):1602.